High-speed In-Situ Tomography of Liquid Protein Foams

Anja Eggert[a], Martina Müller[b], Frank Nachtrab[a], Jannika Dombrowski[c], Alexander Rack[d] and Simon Zabler[a,b]

[a]Development Centre X-ray Technology (EZRT), Fraunhofer Institute for Integrated Circuits (IIS), Fuerth, Germany

[b]Chair of X-ray Microscopy (LRM), Physics and Astronomy, University Wurzburg, Wurzburg, Germany

[c]Chair for Food Process Engineering and Dairy Technology, TU München, Freising, Germany

[d]European Synchrotron Radiation Facility (ESRF), Grenoble, France

Keywords: protein foams; high speed CT; micro tomography; synchrotron; X-ray imaging

Abstract

For the engineering of foamed food products, knowledge about the foam micro-structure as well as about its dynamics and stability are of critical importance to the quality and sensorial perception of the product. Using fast micro-CT in the laboratory as well as ultra-fast in situ phase-contrast synchrotron CT at the European Synchrotron Radiation Facility accurate information about the entire pore distribution in lactic protein foams is obtained almost instantaneously. This study displays the four-dimensional structural dynamics of milk-protein foam decay over time with unparalleled temporal and spatial resolution of the measurement data (2*s* scan time at 2.7 *µm* voxel sampling). 3D volume data processing and pore size analysis down to single pores of 50 *µm* size is applied to a 15 minutes cine-tomography series monitoring the 4D time decay of β-lactoglobulin foam, providing new insights into the dynamics of liquid protein foams.

1. Introduction

Protein foams and, in particular, foams, which are stabilized by the milk proteins β-Lactoglobulin and micellar casein, play an increasingly important role in modern food industry: i.e. for the development of foamed nutritious products. For the latter, the pore size distribution and the structural stability of the foam over time are the key material parameters, whereby micro-foams with a very fine porosity and a very slow coarsening rate are generally preferred. The foam stabilizing abilities of milk proteins make them a very good candidate for engineering food products. To improve these products, a better understanding of the relationship between the production process and the structural properties of the foam is essential. (Lim et al. [1])

Because appropriate quantitative methods are not readily available up today, the structural characterization of liquid foams, which feature structural changes, is still difficult (e.g. milk protein foams decay already after 10-15 minutes) (Lim et al. [1]).

Fast X-ray micro computed tomography (μ-CT) appears to be the perfect solution for the task at hand. μ-CT is a non-invasive 3D imaging technique which can achieve a spatial resolution of few micrometers and less (Bonse et al. [2]). From the 3D data quantitative geometric information of the micro-structure of foams can be measured directly, so that pore size, diameter, shape as well as cell wall thicknesses can be analyzed accurately and with sufficiently large statistics [3, 4, 5], serving as input to numerical modelling of the structural dynamics (Liebscher et al. [6]). With current state-of-the-art technology the authors have already demonstrated a μ-CT acquisition rate of 8 s per scan for foams (Zabler et al. [7]).

Because the requirements for non-invasive three-dimensional in situ characterization of protein foams are very difficult to meet for standard laboratory-based X-ray μ-CT, using a synchrotron light source is the only option to reduce the measurement time to one second or less while maintaining a resolution of 10 μm or less. Using synchrotron μ-CT, Babin et al. [8] recently observed successfully the changes in the cellular structure of bread during baking.

In this study a laboratory and a synchrotron μ-CT setup were used to characterize protein foams with applied image processing and volumetric data evaluation in order to calculate the quantitative descriptors for every single pore. As a representative system to be used for the development of the characterization procedure, milk and

β-lactoglobulin foam are chosen. Apart from mere pore size distribution, the foams time dependent structure is investigated, in order to gain insight into the dynamics of milk protein foams.

2. Material and Methods

2.1. Laboratory-based *μ*-CT

For this foaming experiment we employed a *μ*-CT setup at the Fraunhofer Development Center X-ray Technology (EZRT) which has already been described by Zabler et al. [7]. The foam is generated in a 8 *mm* wide glass column and images are recorded at time points of 2 *min*, 4 *min* and 6 *min* after the initial foaming process. The column is scanned with continuous sample rotation (fly-by) over 180°. Depending on the rotation speed, CT volumes can thus be recorded in scan times down to 8 *s* for a volume of 512^3 voxels (389 projection images). The foam structure is thereby recorded with an effective voxel sampling of 17 *μm* and a spatial resolution of ca. 70 *μm*.

2.2. Milk foam

For the laboratory X-ray *μ*-CT scans a commercial cellular food product was studied (liquid milk foam from an aerosol bomb). This foam features a moderate decay time and relatively thick cell walls, as compared to the protein foams described next.

2.3. Synchrotron phase-contrast *μ*-CT

Synchrotron phase-contrast *μ*-CT was used during the dedicated beamtime MA1548 on the ID-19 imaging beamline at the European Synchrotron Radiation Facility (ESRF) in Grenoble, France.

From the previous laboratory experiment which predicted pore sizes as large as 0.5 *mm* we decided that a larger diameter of the foaming column (2 *cm*) was essential to study the foam decay in situ. Fortunately, ID19 provides a sufficiently large and coherent beam to illuminate a 2 *cm* x 1*cm* field of view (FOV). To maximize the photon flux and minimize the scan time a special undulator source was inserted: a so called single harmonic undulator which features non-periodic pole pairs and has its peak emission at ~19 *keV* thus providing a “pink beam” of 5 *cm* x 1 *cm* size (actually defined by the exit window of the vacuum path). To record high-resolution images at 1 *kHz* full frame-rate, we used a CMOS camera (pco.DIMAX, 2016 x 2016

pixels, PCO GmbH, Germany) coupled to an X-ray scintillator (a 1 *mm* thick scintillating fiber optical plate (sFOP) for 11 *µm* pixel size, hence 1:1 optics, and a 300 *µm* thick LuAG:Ce single-crystalline disc for the 2.7 *µm* voxel size (1:4 optics)). Note that the 1:4 optics yields a high-resolution, region-of-interest CT of the inner foam structure. To enhance the visibility of the foam cell walls by means of inline X-ray phase-contrast the detector was placed 1 *m* downstream of the sample (for the large FOV), 20 *cm* for the high-resolution mode respectively. To avoid artifacts caused by radial acceleration of the foam, the sample rotation axis limit was set to $90° s^{-1}$, yielding a detector frame rate of 500 *Hz*. Hence, for 1000 projections (2016 x 1072 FOV at 1 *ms* exposure; or 2016 x 2016 FOV at 2 *ms* exposure for the 1:4 optics) all scans were acquired within 2 *s* time. Because the foaming took place outside of the experimental hutch, and the column had to be carried to the stage, then the X-ray hutch had to be sealed, the first scan started at 3min time. For each of the foams *µ*-CT scans were recorded at time points of 3 *min*, 5 *min*, 7 *min*, 10 *min* and 15 *min*. After 15min the foam structure appeared sufficiently decayed to stop the measurement.

2.4. β-Lactoglobulin foam

For the faster synchrotron measurements β-lactoglobulin (BLG) protein-foam was chosen for its good foaming properties. It is a model system for the investigation of milk protein foams. The foam is produced on site second before the experiment by a foaming apparatus using the aeration method of Waniska and Kinsella [9].

The protein BLG was refined with a purity of 99.84% from an isolate of whey proteins (WPI 895, Fonterra, New Zealand) using a method described by Toro-Sierra et al. [10]. BLG powder was dissolved in deionized water to yield a protein concentration of 1% (w/w). To ensure full hydration, the dispersion was stirred overnight. For the present study, because BLG is known to be least stable at pH 3, the pH of the solution was set to this very point by adding 1 *M* Hydroclorid acid (HCl). The temperature of the solutions was constant around 20 ℃.

For the foaming process, a DFA100 - Dynamic Foam Analyzer – unit from Krüss GmbH Germany was used. The system is based on the aeration method introduced by Waniska and Kinsella [9]. 10 *ml* of the solution are filled in the sample container. The solution is foamed for 20 *s* by injecting compressed air at 1.5 *bar* pressure

(0,065 l_n min^{-1}) through the floor of the vial which is a porous ceramic membrane with a pore diameter of 9 - 16 *µm* (G4 porosity). Afterwards the pillar with the foam is taken out of the apparatus and directly placed in the CT-System. The same process is carried out three times in order to estimate the reproducibility of the foaming process.

2.5. Data processing and analysis

Prior to tomographic reconstruction the radiographic images were filtered with the ANKAPhase software (version 2.1beta3, cf. Weitkamp et al. [11]) which includes image restoration by means of deconvolution with a Gaussian kernel, combined with single-distance phase retrieval according to Paganin [12]. The phase-radiographs were then processes by a filtered back-projection (FBP) using the program PyHST (Mirone et al. [13]). Figure 1 shows a photo of the sample along with a typical slice from the CT-volume data.

Fig. 1: (a) Photograph of the sample cylinder (PMMA with 2 *cm* inner diameter). (b) FBP reconstructed slice of the protein foam (inset shows magnified view). Scale bar equals 2 *mm*.

The structural analysis of the foam is detailed in Fig. 2. First the volume images are binarized by applying a hysteresis threshold combined with a recursive snow filter. Thereby, the original 8-bit gray-value image is first binarized at a relatively bright grey level (thus creating seeds for the hysteresis), and - after removal of all foreground objects smaller than 100 voxels (snow filter) - a stepwise growth is performed based on descending integer grey levels - until a defined (low) grey level threshold is reached. This method avoids the erroneous selection of brighter voxels not belonging to the cell walls, yet it fails at segmenting the very thinnest walls which are not in contact with one of the seeds during the first step of the binarization. For retrieving the latter, the resulting binary 3D images are segmented using an Euclidean distance transformation and an adaptive water-shedding algorithm from the Software ToolIP (Tool for Image Processing, Fraunhofer ITWM, Kaiserslautern, Germany). Single pores down to 50 *µm* diameter are thus segmented, labelled and analyzed in terms

of position, size, surface, volume and shape. Based on this data histometric pore size distributions can be calculated.

Fig. 2: Pivotal steps in the image processing chain shown for the central slice: (a) binarization of the original image, (b) the binary image serves as input for the distance transformation and (c) the watershed image masked with (a) to obtain the resulting label image. [14]

For the high-resolution synchrotron μ-CT series (BLG at *pH* 3.0) individual growth and shrinkage of a select pore cluster was analyzed, which coalesced at the latest time point (15 *min*) into one single pore. Starting from the latter a 3D mask was created by which the coalesced pores were identified in the previous time step, and so on until the initial pore ensemble was determined at t = 3 *min*. Prior to this 3D masking-and-finding procedure it was necessary to register all 5 datasets in polar coordinates so that central coordinates of corresponding pores would match. This registration is performed manually using the software ImageJ.

3. Results

3.1. Milk foam decay measured with the laboratory μ-CT system

Figure 3 shows the 3D rendering of the milk foam as it decays over time. Note that some of the pore cell walls in the foam can't be distinguished in the isosurface rendering because they are too thin to be detected by the imaging system which is strongly limited in spatial resolution. While the porosity near the column wall remains relatively stable over time a large macro-pore grows at the center of the cavity rising and consuming the smaller surrounding pores until only a thin liquid layer separates the bottom from the top of the column. Note, that for reasons of limited detector size and pixel-binning the column diameter had to be kept down to 8 mm. After two more minutes the remaining layer breaks and the remaining milk foam pours down the sample container walls (Fig. 3c). Volumetric analysis of the smaller pores which prevail after this singular event reveals that despite a rapidly shrinking number of pores the pore size statistic does not change significantly over the entire series, i.e. the average pore diameter as well as the size distribution remain more or less the

same (data shown in Zabler et al. [7]). Additionally, it has to be mentioned that hardly any pores with an ESD (Equivalent Sphere Diameter) below 250 *µm* could be analyzed, hence any structural changes below this threshold remain obscure.

Fig. 3: series of CT images of milk foam decay, recorded at time intervals of 2 *min*.

3.2. Synchrotron

Figure 4 displays the image quality of the laboratory *µ*-CT scan and the quality of the synchrotron *µ*-CT in comparison. Not only is the spatial resolution of the CT slices visibly improved (estimated 30 *µm* for the synchrotron vs. estimated 70 *µm* FWHM blurring for the laboratory setup), but the image contrast between cell walls and air makes the largest difference, and this despite the fact that the cell walls of the milk foam are visibly thicker than those made of pure BLG solution. Note, that also the pore size distribution is visibly different between the two images, with the synchrotron slice showing a far more homogeneous porosity, while the milk foam is clearly more inhomogeneous, an effect most probably caused by the boundary condition due to the much smaller foaming column. In contrast to the laboratory *µ*-CT even the thinnest cell walls are clearly outlined in the phase retrieved synchrotron data thanks to the phase contrast signal which is particularly sensitive to material interfaces.

Fig. 4: CT images of milk foam recorded by a laboratory CT system (left) and of BLG foam recorded with synchrotron phase contrast CT (right).

Figure 5 shows synchrotron *µ*-CT slice from the binarized data corresponding to five time points (3 *min*, 5 *min*, 7 *min*, 10 *min* and 15 *min*) of the BLG foam decay. The coarsening as well as the general structural changes can be readily observed in this sequence. While pore coalescence appears to take place mostly for the very large pores (ESD > 1 *mm*), the smaller pores display only faint growth or shrinkage mostly perceived as the reorientation and shifting of the entire pore ensemble. Also a continuous thinning of the pore cell walls (drainage) can be observed marked by a stronger contrast of the triple joints. Clearly these 2D images are not sufficient to foster more conclusions, which is why analytic 3D morphological analysis was

applied to all pores in the volume. The histometric pore size distribution (number of pores vs. ESD) of the BLG foam is shown in Fig. 6 for all 5 time steps.

Fig. 5: Sequence of binary axial CT slices of BLG foam at pH 3.0.

Unlike what has been observed from the laboratory μ-CT scan (percentage size distribution did not change), Fig. 6 shows the number of larger pores (ESD > 0.9 *mm*) to rise and the number of the smaller pores to shrink (ESD < 0.9 *mm*). The number of pores which have an ESD close to this transition point (~ 0.9 *mm*) meanwhile remains relatively constant over time. Integration of the histograms in Fig. 6 reveals that the average pore ESD increases from 0.337 *mm* (at 3 *min)* to 0.389 *mm* (at 15 *min)* which is quite moderate compared to the growth rate of the largest bubble which almost doubles its ESD during the same time (from 4.9 *mm* to 8.3 *mm,* cf. Table 2). During the whole sequence, the number of pores decreases monotonously, which is apparently caused by the vanishing of the smallest pores (ESD < 0.1 *mm*).

Fig. 6: Time development of pore size distribution of BLG foam at pH 3 over 15 *min*.

Table 1: Statistical results of the BLG foam structure.

Recording a BLG foam in high-resolution ROI μ-CT at the ESRF we obtained a more detailed view onto a small ensemble of pores, from which one pore cluster was selected (images taken at different times, are shown in Fig. 7. This cluster was selected after data registration and 3D masking in order to define those pores which vanished during the series in order to merge into a single large pore at t =15 *min* (Fig. 7d). While at the starting point (5 *min*, cf. Fig. 7a) the cluster consists of more than 100 pores, these 101 become 85 after 7 *min*, and one single pore after 15 min. With the exception of the last two time steps (10 *min* and 15 *min*) the structural changes in the ensemble appear to be subtle, hence it is necessary to investigate the growth/shrink rate of each pore individually.

Fig. 7: Development of a foam cluster over 15 *min*.

Therefore, three random pores (labeled with their numbers in Fig. 7) in the cluster are selected for individual investigation. Single pore size evolution for these examples is displayed in Fig. 8. As mentioned earlier, pore no. 1, which is large pore, consumes the complete ensemble at 15 *min* and shows a constant very fast growth rate of ca. 0.7 mm^3/min, reaching 12.4 mm^3 size at t = 15 *min*. On the other hand pore no. 2 is much smaller from the start and actually decreases in size starting with 0.054 mm^3 volume at t = 3 min and descending to 0.039 mm^3 at t = 10 *min* before it coalesces with pore no. 1. Pore no. 3 belongs to a size range between no.1 and no. 2 and shows a moderate volume increase from 0.49 mm^3 at t = 3 *min* to 0.57 mm^3 (15 min). The growth rate for all three pores appears to be more or less constant (linear).

Fig. 8: Pore volume development of three pores (numbered in Fig. 7) over 15 *min*.

4. Discussion

The time-evolution of liquid and semi-liquid protein foams as reported in this study represents the spear tip of what is possible with today's 3D measurement techniques, both in terms of spatial and temporal resolution. While in laboratory CT faster scan times are generally achieved by sacrificing on the spatial resolution, hence on the microscopic detail of the volume data, both high spatial resolution and short scan times can be combined on a synchrotron beamline simply thanks to the high brilliance of the available X-ray beam. This is particularly important for the class of liquid foams from which we studied milk and milk protein foams, which feature a very broad pore size distribution: pores from 50 μm to 5 *mm* had to be measured in a sufficiently large volume (2 *cm*).

For the BLG scan times of 1 *s* or 2 *s* were a stringent requirement to measure the foam in its native state, while assuming a quasi-stationary structure which does not change during the scan. Any changes, hence violations of the stationary condition have been observed to add artifacts to the reconstructed 3D volume and obscure the measurement. In contrast to the synchrotron scans, the lab CT scans shown in this study required the addition of stabilizing factors to the protein solution in order to maintain a stable foam structure over 8 – 15 *s* time. For both cases, the changes we observed in the foam structure between two timeframes were significant and it is

highly desirable for future tests to achieve repeat cycles for 3D scans that are shorter than the 2 – 5 *min* delay which were applied in this study. 2 minutes was actually the time required to transfer one set of projection images (one scan) from the camera RAM to the hard drive. This delay can be overcome by realizing a continuous data spooling.

Synchrotron facilities provide a highly brilliant X-ray beam, thus allowing for scanning times and data quality which cannot be achieved (at least not simultaneously) with laboratory X-ray sources. Using high-precision fast rotation and a CMOS sensor, a complete μ-CT scan is recorded in one or two seconds. The air-liquid interface contrast is thereby greatly improved by the formation of phase contrast in the images. Using ToolIP software from Fraunhofer ITWM for the image analysis we are able to extract geometric and structural parameters of every single pore in the volume. When the synchrotron setup is employed in high resolution mode the FOV is restricted to a few hundred pores, but one the other hand the geometry of the smallest pores is more accurately reproduced. Therefore, in order to study a limited ensemble of pores in a cluster – and, possibly referring the growth rate of each individual pore to its neighbors, following the way we here demonstrated for three pores - this imaging mode is preferred.

Regarding the non-invasive nature of the technique it has to be mentioned that the Plexiglas vial through which the foams were measured at the synchrotron, first developed a yellow color under the radiation, then after 10 – 12 hours the material formed a network of fine hair cracks which caused the structure to collapse. Despite the fact that the X-ray absorption by the water-protein solution which forms the cell-walls is very little and of the order 10^{-4}, the effective dose during a single scan can be as high as 10^5 *Gy* (Langer et al. [15]). During the scans we did not observe a structural behavior of the irradiated foam that was significantly different from the non-irradiated parts. When comparing the solution's pH before and after the scans did not reveal any change which would indicate a major increase in free radicals from the ionization. With appropriate precaution we therefore hypothesize that the structural decay of the foam was not influenced by radiation effects, at least not on a measurable time and length scale.

In order to assess the error of the measurement introduced by the image processing chain of the ToolIP analysis software, artificial closed foam was simulated consisting

of well-defined hollow spheres. This simulation included forward projection and Fresnel-propagation, as well as filtered back-projection and phase retrieval. Applying the same analysis to this phantom volume revealed that the pore diameters are slightly under-estimated; hence have to be corrected by 10 – 15 % for the smallest pores and 3 – 5 % for the larger pores in the volume. Since the outcome of the analysis depends strongly on the H-min transformation which is applied between the EDT and the watershed, alternative methods might be considered in the near future, possibly taking into account the triple joints and facilitating the closure of the cell walls.

Reproducibility of the foam structure appears to be mostly limited by small contaminations of the protein solution caused by using the same vial for all experiments, as well as by demixing of the solution when it was used some time after the mixing procedure. In order to predict the foaming behavior more accurately from such measurements, one will have to work on the suppression of these effects.

5. Conclusion

With the sub-µ CT-System at the Fraunhofer EZRT it is possible to realize scan times down to 8 *s* for a 3D volume of 512^3. This allows for the investigation of moderately stable foams, like milk. Yet more instable systems, as well as systems with a lower viscosity of the liquid phase cannot be measured in the laboratory *µ*-CT system because of an insufficient spatial and temporal resolution. Another drawback of the laboratory system, which becomes apparent from our results, is the fact that milk or protein solutions have a very low X-ray attenuation compared to air, hence the image contrast of the µ-CT scans is very poor and perturbed by strong photon noise.

As we demonstrated, the quality of protein foam scans is highly improved through the use of a brilliant X-ray beam as is the case at a synchrotron light source, allowing for high speed scans and phase contrast. The X-ray beam was therefore optimized both for size, homogeneity and flux rather than for reduced bandwidth. Hence, a pink configuration (without monochromator) was used for the experiment with a diamond window and Be window as the only mandatory optical components in the beam path. Phase contrast and numerical phase retrieval proved to be robust to these violations of the boundary conditions which are generally assumed for phase techniques, i.e.

high spatial detector resolution and a narrow energy bandwidth of the beam. Phase maps were successfully retrieved from radiographs which are recorded with a sFOP screen, sampled at 11 *µm* pixel size and an approximate point spread of 30 *µm*. The high brilliance is thus mainly used for working at a very low beam divergence, hence a fairly good partial transversal optical coherence.

In the field of food technology, *µ*-CT has already been successfully applied to study the porous structure of dried banana slices (Léonard et al. [16]), yeast (Debaste et al. [17]), wheat flour dough (Bellido et al. [18]), and the microstructure of processed meat (Frisullo et al. [19]) as well as various other porous food products (Lim et al. [1]). Yet, all samples which were measured in these studies did not change their structure over a short time. “Short” meaning the acquisition time which is required for a typical µ-CT scan: 10 min to 1h 20 *min*. During the µ-CT scan the sample micro-structure has to remain stable over time otherwise the volume information is destroyed by strong imaging artifacts. Consequently, successfully applying µ-CT to liquid and semi-liquid foams requires much shorter scan times in order to fulfill this assumption. The time constant over which protein foams remain globally stable is several minutes, yet structural changes (displacement, coalescence, coarsening) at the level of single pores occurs within seconds or less. µ-CT has the big advantage, compared to other methods, that the technique is non-invasive, i.e. the object is not influenced through the procedure. This way the same sample can be investigated several times and its behavior can be observed over time.

We thank Dr. Katja Schladitz (ITWM) for her generous support and assistance with the ToolIP software. Markus Kiunke from the Chair of X-ray microscopy shall be honored for reconstructing and binarizing more than 660 volume data sets by using parallel computing. The research project AiF 17124 N was supported by the German Ministry of Economics and Technology (via AiF) and the FEI (Forschungskreis der Ernährungsindustrie e.V., Bonn). The authors gratefully acknowledge the funding of the German Research Council (DFG), who, in the framework of the “Excellence Initiative” supports the Cluster of Excellence ‘‘Engineering of Advanced Materials’’ at the University of Erlangen-Nürnberg. These studies were further co-financed by the free state of Bavaria. The Authors thank the ESRF for granting beamtime at beamline ID19 in frame of proposal MA1548.

References

[1] K. S. Lim, M. Barigou: X-ray micro-computed tomography of cellular food products, Food Research International, 37 (2004) 1001–1012, doi: 10.1016/j.foodres.2004.06.010.

[2] U. Bonse, F. Busch: X-ray computed microtomography (µCT) using synchrotron radiation (SR), Prog. Biophys. Molec. Biol. 65 (1996) 133-169, doi: 10.1016/S0079-6107(96)00011-9.

[3] A. Heuer, A. R. Coxa, S. Singleton, M. Barigou, M. van Ginkel: Visualisation of foam microstructure when subject to pressure change, Colloids and Surfaces A: Physicochem. Eng. Aspects, 311 (2007) 112–123, doi: 10.1016/j.colsurfa.2007.06.004.

[4] C. Redenbach, A. Rack, K. Schladitz, O. Wirjadi, M. Godehardt: Beyond imaging: on the quantitative analysis of tomographic volume data, International Journal of Materials Research, vol. 103, no. 2 (2012) 217-227, doi: 10.3139/146.110671

[5] A. Rack, L. Helfen, T. Baumbach, S. Kirste, J. Banhart, K. Schladitz, J. Ohser: Analysis of spatial cross-correlations in multi-constituent volume data, Journal of Microscopy, vol. 232, issue 2 (2008) 282-292, doi: 10.1111/j.1365-2818.2008.02100.x

[6] A. Liebscher, C. Redenbach: 3D image analysis and stochastic modelling of open foams, International Journal of Materials Research, vol. 103, no. 2 (2012) 155-161, doi: 10.3139/146.110667

[7] S. Zabler, C. Fella, A. Dietrich, F. Nachtrab, M. Salamon, V. Voland, T. Ebensperger, S. Oeckel, R. Hanke, N. Uhlamnn: High-resolution and high-speed CT in industry and research, Proc. SPIE vol. 8506 (“Developments in X-Ray Tomography VIII”), 850617 (2012), doi:10.1117/12.964588

[8] P. Babin, G. Della Valle, H. Chiron, P. Cloetens, J. Hoszowska, P. Pernot, A. L. Réguerre, L. Salvo, R. Dendievel: Fast X-ray tomography analysis of bubble growth and foam setting during breadmaking, Journal of Cereal Science, 43 (2006) 393–397, doi: 10.1016/j.jcs.2005.12.002.

[9] R. D. Waniska, J. E. Kinsella: Foaming properties of proteins: evaluation of a column aeration apparatus using ovalbumin, Journal of Food Science, 44 (1979) 1398–1411, doi: 10.1111/j.1365-2621.1979.tb06447.x

[10] J. Toro-Sierra, A. Tolkach, U. Kulozik: Fractionation of α-Lactalbumin and β-Lactoglobulin from Whey Protein Isolate Using Selective Thermal Aggregation, an Optimized Membrane Separation Procedure and Resolubilization Techniques at Pilot Plant Scale, Food and Bioprocess Technology, 6 (4) (2013) 1032-1043, doi: 10.1007/s11947-011-0732-2

[11] T. Weitkamp, D. Haas, D. Wegrzynek, A. Rack: ANKAphase: software for single-distance phase-retrieval from inline X-ray phase contrast radiographs, Journal of Synchrotron Radiation, 18 (2011) 617–629, doi: 10.1107/S0909049511002895

[12] D. Paganin, S. C. Mayo, T. E. Gureyev, P. R. Miller, S. W. Wilkins: Simultaneous phase and amplitude extraction from a single defocused image of a homogeneous object, Journal of Microscopy-Oxford, 206 (2002) 33-40, doi: 10.1046/j.1365-2818.2002.01010.x

[13] A. Mirone, E. Gouillart, E. Brun, P. Tafforeau, J. Kieffer: PyHST2: an hybrid distributed code for high speed tomographic reconstruction with iterative reconstruction and a priori knowledge capabilities, Nucl. Instrum. Meth. B, in press (arXiv:1306.1392).

[14] A. Eggert, J. Dombrowski, S. Zabler: Characterization of Instable Food Foams Using Fast Micro-CT in a Laboratory Setup and at a Synchrotron Source, InsideFood Symposium, 9.-12. April 2013, Leuven, Belgien (2013)

[15] M. Langer, A. Pacureanu, H. Suhonen, Q. Grimal, p. Cloetens, F. Peyrin: X-Ray Phase Nanotomography Resolves the 3D Human Bone Ultrastructure, Plos One, Vol. 7, Issue 8, e35691

[16] T. Léonard, S. Blacher, C. Nimmol, S. Devahastin: Effect of far-infrared radiation assisted drying on microstructure of banana slices: An illustrative use of X-ray microtomography in microstructural evaluation of a food product, Journal of Food Engineering, 85 (2008) 154–162, doi: 10.1016/j.jfoodeng.2007.07.017.

[17] F. Debaste, A. Léonard, V. Halloin, B. Haut: Microtomographic investigation of a yeast grain porous structure, Journal of Food Engineering, 97 (2010) 526-532, doi: 10.1016/j.jfoodeng.2009.11.012.

[18] G. G. Bellido, M. G. Scanlon, J. H. Page, B. Hallgrimsson: The bubble size distribution in wheat flour dough, Food Research International, 39 (2006) 1058–1066, doi: 10.1016/j.foodres.2006.07.020.

[19] P. Frisullo, J. Laverse, R. Marino, M. A. Del Nobile: X-ray computed tomography to study processed meat microstructure, Journal of Food Engineering, 94 (2009) 283-289, doi: 10.1016/j.jfoodeng.2009.03.020.

Correspondence address

M. Sc. Anja Eggert
Fraunhofer-Entwicklungszentrum Röntgentechnik EZRT
Flugplatzstraße 75, 90768 Fürth, Germany
Tel.: +49 911 58061-7664
Fax: +49 911 58061-7599
e-mail: anja.eggert@iis.fraunhofer.de

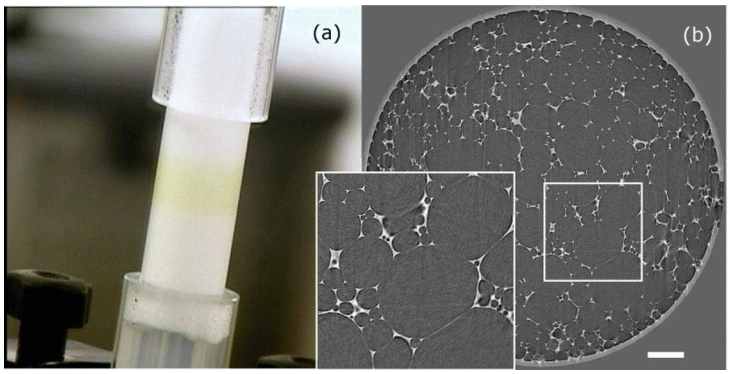

Fig. 1

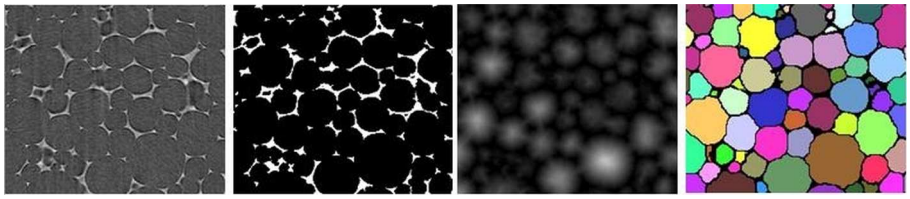

Fig. 2

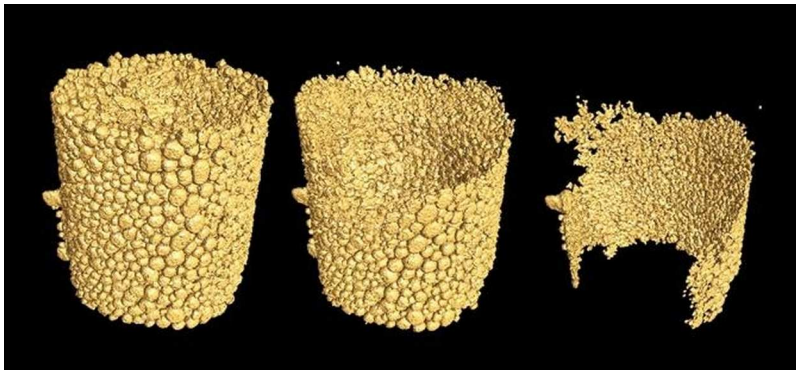

Fig. 3

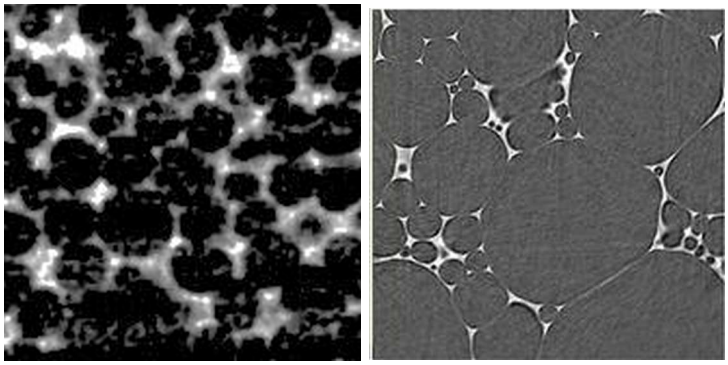

Fig.4

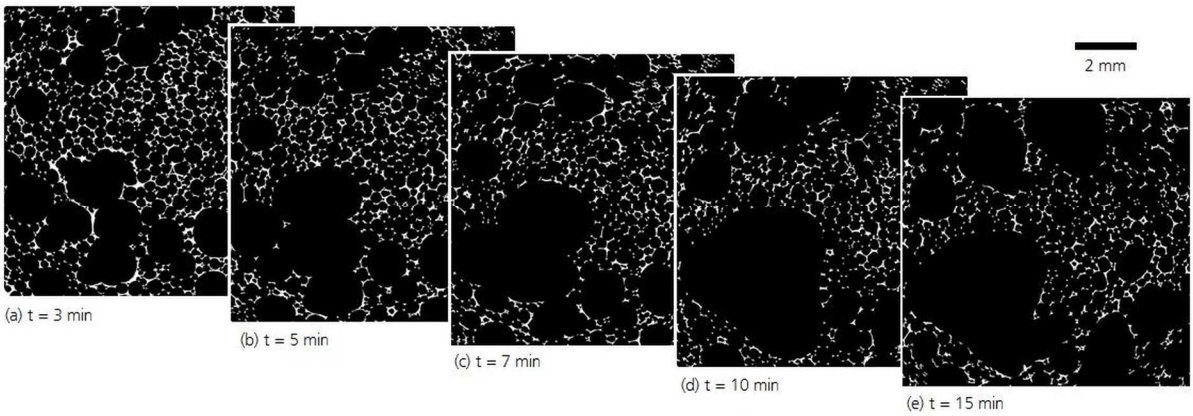
2 mm
(a) t = 3 min
(b) t = 5 min
(c) t = 7 min
(d) t = 10 min
(e) t = 15 min

Fig. 5

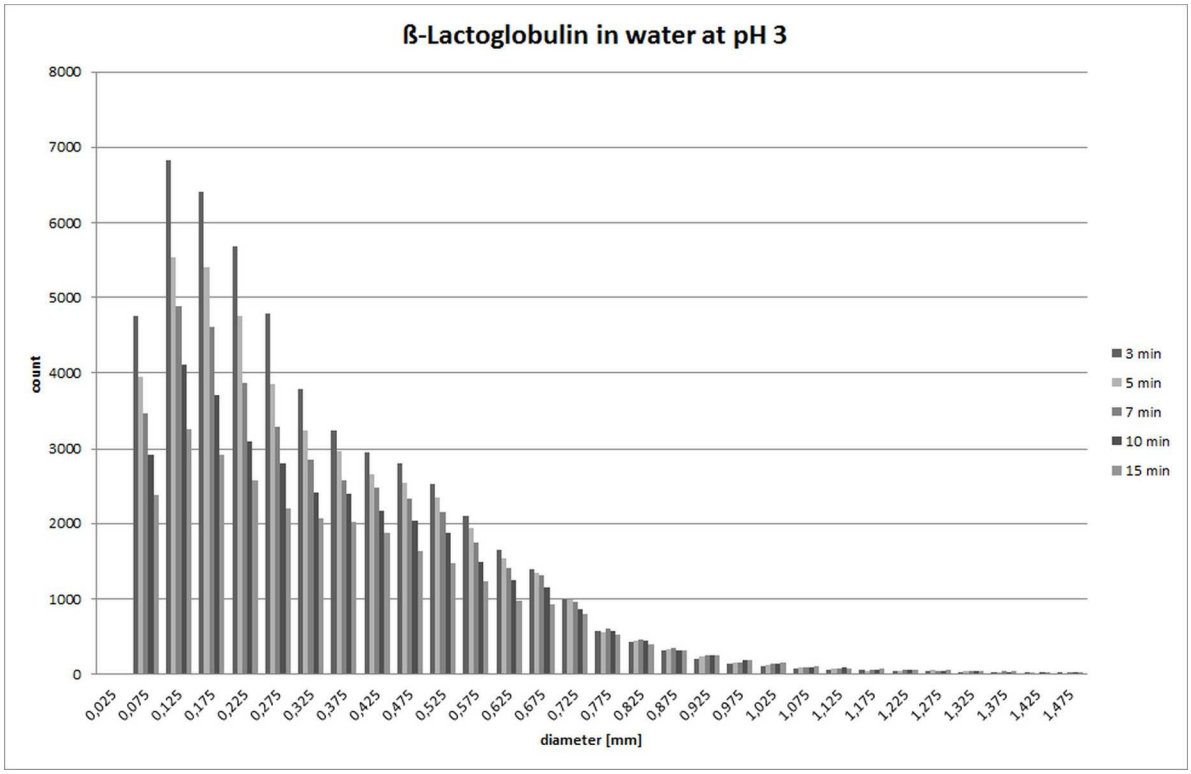
ß-Lactoglobulin in water at pH 3
count
diameter [mm]
3 min
5 min
7 min
10 min
15 min

Fig. 6

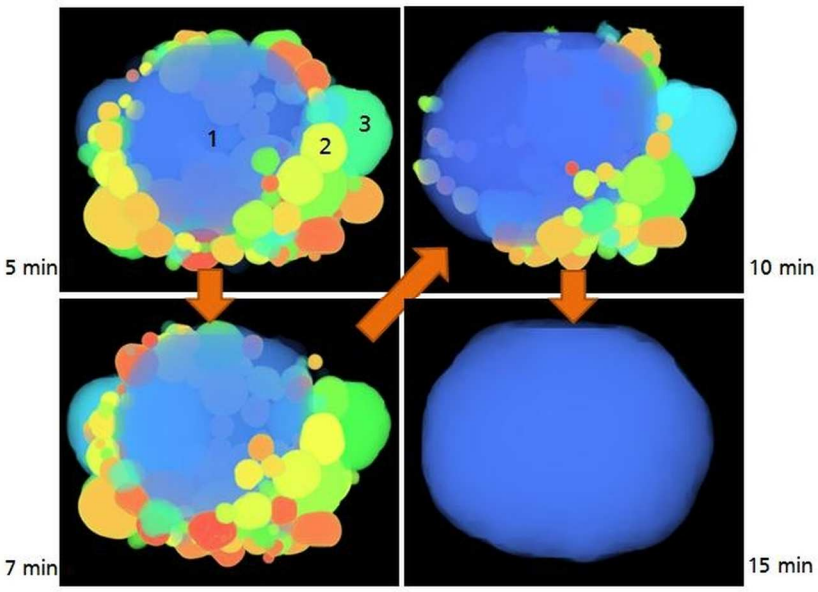

Fig. 7

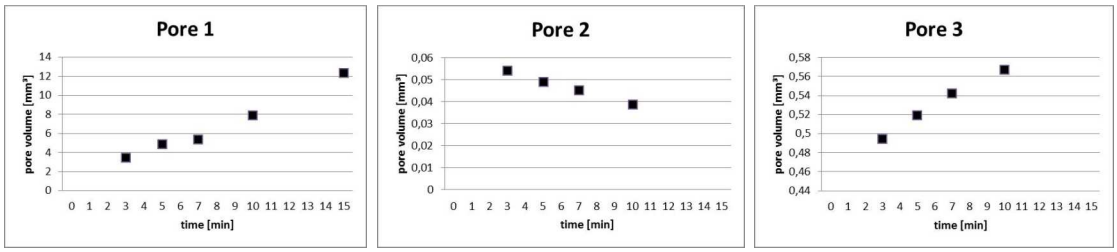

Fig. 8

	3 min	5 min	7 min	10 min	15 min
Number of pores	52310	45617	40612	34917	28910
Average pore diameter *[mm]*	0,337	0,353	0,365	0,376	0,389
Standard deviation *[mm]*	0,245	0,259	0,271	0,282	0,301
Minimum *[mm]*	0,055	0,055	0,055	0,055	0,055
Median *[mm]*	0,275	0,290	0,303	0,315	0,326
Maximum *[mm]*	4,908	4,811	5,841	7,786	8,276

Tab. 1